# We are IntechOpen,
## the world's leading publisher of Open Access books
## Built by scientists, for scientists

**6,900**
Open access books available

**185,000**
International authors and editors

**200M**
Downloads

**154**
Countries delivered to

Our authors are among the

**TOP 1%**
most cited scientists

**12.2%**
Contributors from top 500 universities

CLARIVATE ANALYTICS
**BOOK CITATION INDEX**
INDEXED

**WEB OF SCIENCE™**

Selection of our books indexed in the Book Citation Index
in Web of Science™ Core Collection (BKCI)

## Interested in publishing with us?
## Contact book.department@intechopen.com

Numbers displayed above are based on latest data collected.
For more information visit www.intechopen.com

# Growth Study and Characterization of Single-Layer Graphene Structures Deposited on Copper Substrate by Chemical Vapour Deposition

Stefanos Chaitoglou, Enric Bertran and
Jose Luis Andujar

Additional information is available at the end of the chapter

## Abstract

Currently, the graphene industry is moving forward to the import of graphene in a number of novel applications. To take full advantage of the excellent properties of the material, the standardization of the growth process is an emergency. The suitable growth technique should ensure the high yield, accompanied by high quality of single-layer graphene sheets. Chemical vapour deposition is the technology that fulfils the above requirements, promoting the growth of largescale graphene films through automatized processes. In the present chapter, we present the latest advances in this field, summarizing the most recent publication activity of the authors. The results outline how the control in the growth process over parameters like the gases flow, growth temperature and pressure can affect the nucleation density of graphene domains, the growth rate and percent coverage. Growth of graphene domains with different morphologies depends on the crystallographic orientation of the copper lattice. At the same time, the formation of ripples occurs in the graphene surface as a result of the copper foil compression during the cooling step. These ripples are responsible for the appearance of a compressive stress in the graphene sheets. We demonstrate the control over such stress through the variation in the hydrogen flow during the growth.

**Keywords:** graphene films, chemical vapour deposition, ripples formation, hydrogen effect

## 1. Introduction

Bottom-up synthesis methods like chemical vapour deposition (CVD) are those that better ensure the growth of continuous graphene films [1]. Evidence of the potential to move to industrial scale synthesis has been proven [2, 3]. When the various graphene nuclei reach the coalescence phase, they join to each other, forming a continuous layer. In this growth model, the grain boundaries are proven defects points affecting the quality of the graphene layer, both concerning mechanical and electrical properties. Thus, it is an emergency to proceed with the growth of wafer-scale single crystal graphene domains [4–10]. Efficient growth approaches should ensure a low nucleation density of graphene domains, followed by high growth rates. Parameters that affect the synthesis process are the gas mixture and growth pressure, temperature and time [11]. Copper foil is one of the preferred substrates for the CVD growth as it permits the production of large-scale, single-layer graphene domains [12]. Carbon atoms show a low solubility into the copper. More carbon species remain in the surface of the foil participating in the formation of the graphene sheet [1]. A conventional CVD growth method consists of a continuous flow of carbon gas precursor/$H_2$/Ar mixture in order to generate the graphene growth [13]. In all experiments described in this chapter, methane is used as carbon precursor. As described in the work of Li et al. [14], the steps for the graphene CVD growth are the following:

1. Exposure of Cu to methane, argon and hydrogen.

2. Catalytic decomposition of methane on Cu to mainly form $CH_y$ species.

3. As a result of the temperature, methane pressure, methane and hydrogen flow and partial pressure, the Cu surface appears undersaturated, saturated or supersaturated with $CH_y$ species.

4. Formation of nuclei as a result of local supersaturation of $CH_y$.

5. Nuclei grow to form graphene islands.

6. Full Cu surface coverage by graphene under specific temperature flow rates and pressure conditions.

The hydrogen presence has proved to play a critical role in the process, as it affects different mechanisms. It reduces the native copper oxide layer and activates the graphene growth. At the same time, it can apply an etching on the material. Thus, it is fundamental to fully understand the above mechanisms. It has been investigated before how hydrogen can affect thickness, shape, size, edge configuration and crystalline quality of graphene islands/domains as well the control of the nucleation density [15–21], which is very important, taking advantage of the low solubility of carbon into copper [21–27]. Polishing of the copper surface or even enclosure of the substrate in special 'pockets', enables the control of the gases mixture, has proven to help in the control of the nuclei density [12]. The use of high growth temperatures favours the copper recrystallization, permitting the growth of high-quality graphene [28]. Searching for means to further reduce the nucleation, it has been proposed the oxidation of

the copper surface [29, 30] resulting in very low domain density with size up to 1 cm$^2$ [31]. In order to reduce the copper surface, thermal annealing processes are usually applied, which require long periods of baking [32].

In this chapter, we present new experiments and results evidencing the effect of the partial pressure of H$_2$ at a given CH$_4$/H$_2$ gas flow ratio on the growth of bi-dimensional crystals of graphene and on their morphology.

To provide a better understanding of the physicochemical mechanisms that govern film formation, we include them in the framework of atomic level phenomena such as adsorption, diffusion and nucleation, providing the possibility to have a full control on the growth process. We study the CVD growth of graphene in the range between 970 and 1070°C, examining the temperature effect in the graphene growth ratio and nucleation density. By fitting the graphene coverage ratio as a function of growth time, we estimate an activation energy of 3.01 eV.

Finally, we study the formation of ripples in the surface of the graphene sheet. Ripples in the graphene surface are proven to affect its electronic structure [33], carrier transport[34] and chemical properties.[35] Therefore, the capability to control the formation of this kind of corrugation is urgent.

In other recent works, Park et al. have demonstrated the capability to control the density and height of such ripples through control of the cooling ratio, which follows the growth step [36, 37]. Slow cooling permits the formation of molecular hydrogen, which can result in the suspension of the graphene film. Moreover, they have demonstrated the importance of such ripple morphology in the mobility properties of the graphene. Graphene with fewer and smaller ripples demonstrates better transport properties when it is embodied in electronic devices.

## 2. Experimental part

The whole process was carried out in a suitable CVD oven (schematically drawn in **Figure 1**). The reactor consists of a furnace, where the CVD process takes place, coupled to a spherical chamber with a magnetron sputtering system. The turbomolecular pump can achieve a vacuum in the order of ~10$^{-4}$ Pa, providing a very pure atmosphere for the graphene growth. This allows us to deposit different thin films (copper-nickel on silicon) in ultrapure conditions (without oxygen) and to perform directly the graphene growth without exposing the substrate to the ambient. By this method, all the treatments, since the cleaning process and reduction/annealing of the copper foil or the deposition of the metal catalyst by sputtering, can be performed '*in situ*' by a single run. For the evaluation of the obtained graphene, we used Raman spectroscopy as well as scanning electron and atomic force microscopy. The scanning electron microscopy (SEM) images were taken with a JEOL JSM7100F microscope in 5 keV. The Raman spectroscopy was performed with a Jobin-Yvon LabRam HR 800 system. A green laser with a 2 μm spot diameter has been used. Atomic force microscopy (AFM) image has been obtained with an AFM Multimode 8, electronica Nanoscope V (Bruker), and operated by the NOVA software.
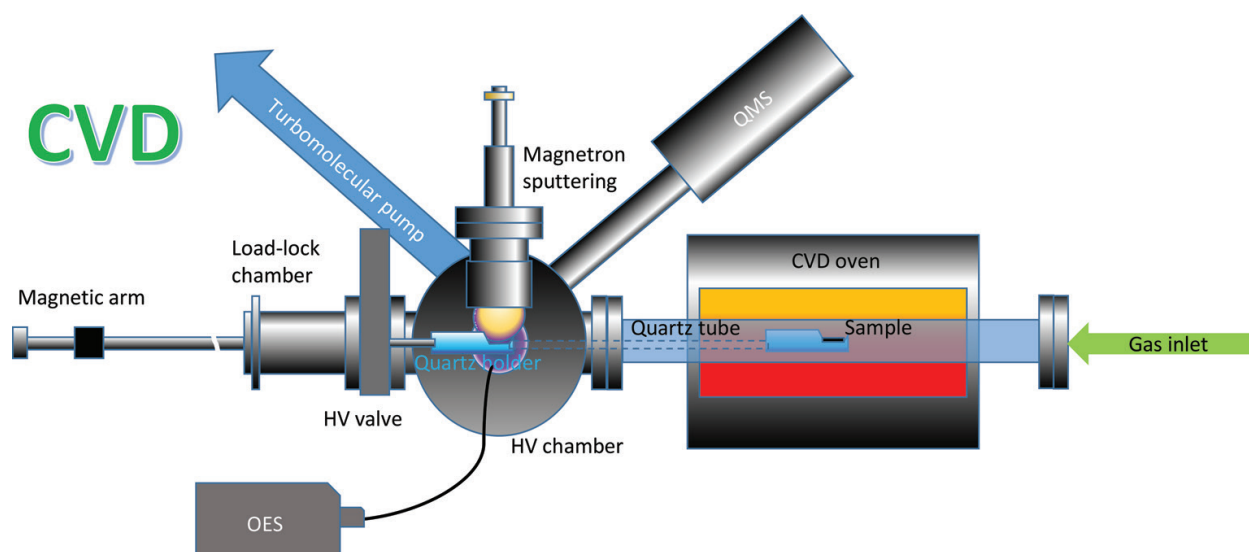
**Figure 1.** Illustration of the reactor. The system consists of two parts, a chamber with a magnetron sputtering head for thin films deposition and a quartz tube where the CVD processes take place.

### 2.1. Pretreatment of copper foil

Polycrystalline copper foil 75 μm thick and 99% pure was cut in pieces of $2 \times 2$ cm$^2$. The foil piece is cut in pieces of $2 \times 2$ cm$^2$. It is pre-cleaned with acetone and isopropanol immersed in an ultrasonic bath for 10 min. Then it is being introduced into the CVD reactor. In other works, the application of argon/hydrogen of helium/hydrogen plasma for the effective pre-treatment of the copper foil is being introduced. Plasma pre-treatment is, moreover, found to improve the crystallinity of the formed graphene [38]. Here we present the performance of hydrogen plasma for the same purpose. From previous studies made in our group [39], we have been able to optimize the parameters necessary to use in order to reduce the native copper oxide layer. According to these results, first, a background pressure of $7 \times 10^{-4}$ Pa is applied with a turbomolecular pump to secure that the whole process is taking place under high purity conditions. Radio frequency (RF) hydrogen plasma is then applied to chemically reduce the copper substrate. To generate the plasma, we introduce hydrogen with 20 sccm flow rate and applied 100WRF power at 20 Pa. The hydrogen radicals react with the copper oxide .

$$CuO + 2H \rightarrow Cu + H_2O \tag{1}$$

### 2.2. Graphene CVD growth

The authors have investigated in various works [40, 41] the growth mechanisms of graphene and the effect of parameters like the hydrogen concentration, growth pressure, time and temperature. The hydrogen flow appears to perform an etching in the graphene domains, which affects their morphology and uniformity, when its concentration exceeds some limits. The results reveal that a sufficient graphene growth is possible when we optimize the switching of the carbon precursor/hydrogen flow ratio during the process. This reduces the etching effect that the hydrogen is performing, allowing the growth of graphene and the full cover of the substrate by it.

We first perform experiments varying the gas mixture ratio, hydrogen/methane and the total pressure. By analysing images obtained by scanning electron microscopy, under stable methane/hydrogen flow rate and varying the total pressure, we study the variation in the nucleation density and size of the graphene domains. Under stable pressure and varying the hydrogen flow, we observe the anisotropical etching that the second performs when its concentration exceed an equilibrium amount

Samples grown under different conditions have been observed by SEM, using the Image J software. The amount of samples analysed can be seen in the size distribution histograms presented in this chapter. We keep a stable methane/hydrogen ratio, 5/20 sccm, and control the total pressure in the chamber by rotating the conductance valve which is placed in the turbomolecular pump. In **Figure 2**, we have the series of samples that were grown at 20 min, in a range of pressures between 12.5 and 20 Pascal. To control the hydrogen effect, we perform growths of the same duration, under stable pressure and methane flow and varying the hydrogen flow in the range between 10 and 20 sccm (**Figure 3**). All the experimental conditions are presented in **Table 1**. To study the size of the graphene domains, we use the length of the lobes.
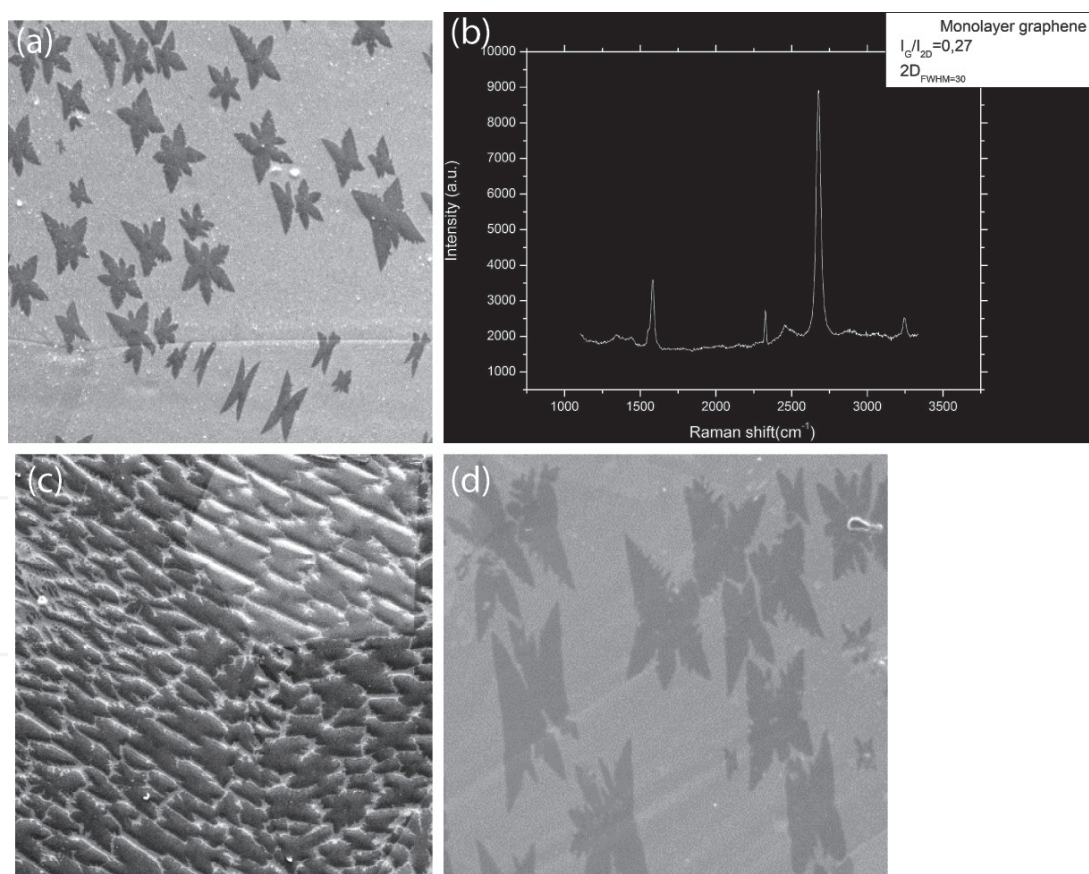


**Figure 2.** Scanning electron emission images of graphene grown in stable methane/hydrogen (5/20 sccm) flows under different total pressures. Figure (a) 12.5 Pa total pressure, (b) 15 Pa, (c) to 17.5 Pa, (d) to 20 Pa. The size of the crystals is dependent on the growth total pressure in a not linear way. In panel (b) is being provided a Raman spectrum of the continuous graphene film after its transfer on top of $SiO_2$. The length of the X direction is 200 μm in all figures.
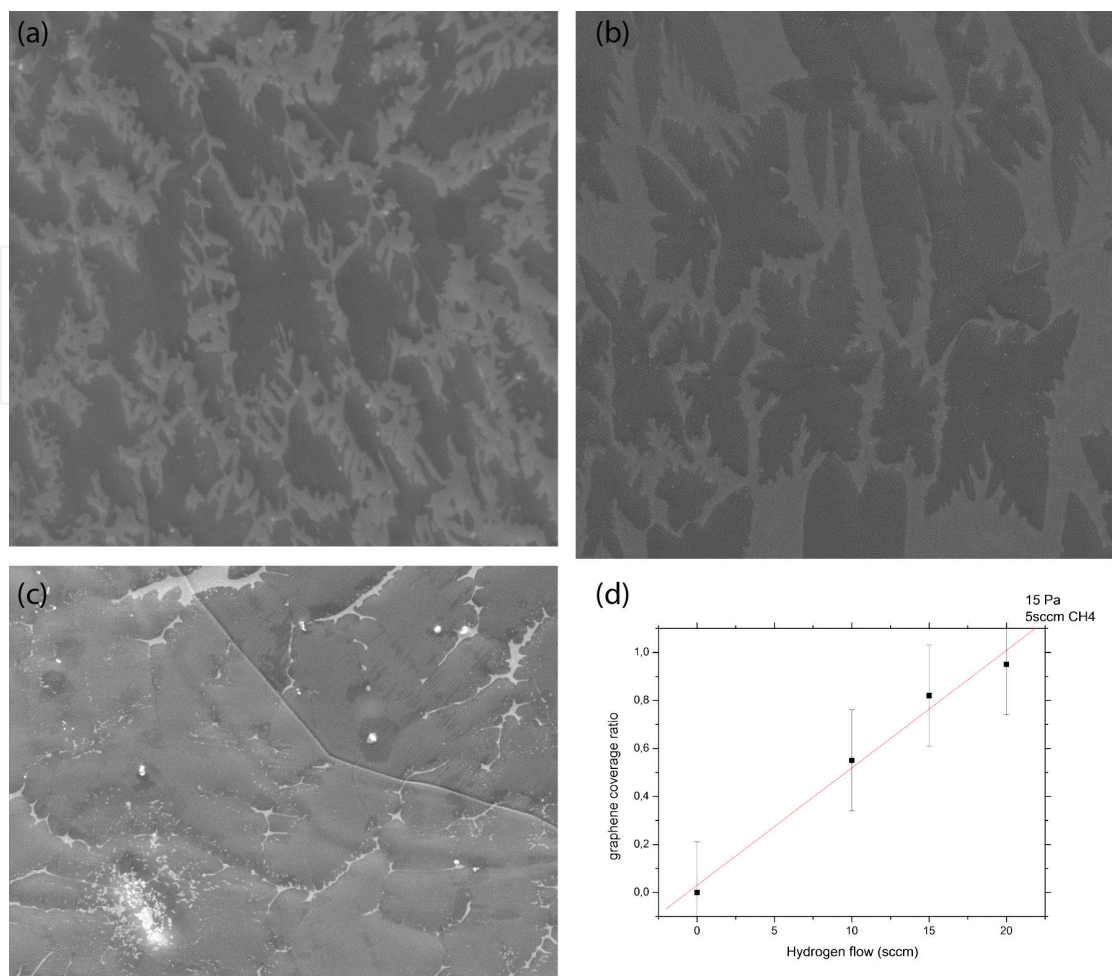
**Figure 3.** Scanning electron microscopy images of graphene grown under 5 sccm of methane, at 15 Pa total pressure, in 1040°C, during 20 min. Varying the hydrogen flow, at (a) 10, (b) 15 and (c) 20 sccm affects the morphology of the film. The scale bar is in all the images 10 μm. In panel (d) the plot demonstrates the percent graphene covered area. The highest coverage, ~95% corresponds to the highest hydrogen flow.

| Sample (corresponding image) | Total pressure (Pa) | Hydrogen flow (sccm) | Crystal's lobe length (μm) | Nucleation density (nucleus/1000 μm²) | % Surface cover |
|---|---|---|---|---|---|
| Image 2a | 12.5 | 20 | 13 | 0.8 | 15 |
| Image 2b | 15 | 20 | 27 | 1.2 (full cover) | 100 |
| Image 2c | 17.5 | 20 | 14 | 3.7 | 82 |
| Image 2d | 20 | 20 | 32 | 0.5 | 40 |
| Image 3a | 15 | 10 | 30.5 | 2.6 | 55 |
| Image 3b | 15 | 15 | 30.1 | 0.8 | 82 |
| Image 3c | 15 | 20 | 27 | 1.3 | 95 |

**Table 1.** Experimental conditions of the samples presented in **Figures 2** and **3**. The methane flow is the same in all experiments, 5 sccm, as well as the growth time (20 min) and temperature is 1040°C. In the table, the effect of growth total pressure and hydrogen flow to the crystal size as well as the nucleation density is presented.

## 2.3. Temperature effect

We investigated the growth of graphene in the range between 970 and 1070°C. Below that temperature graphene nucleation was not observed, while the upper limit was chosen in order to be as close as possible to copper melting temperature (1084°C). The rest of the growth process is followed as explained in the previous chapter. The pressure is stable at 15 Pa and the $CH_4/H_2$ = 5/20. The only varying factor is the growth temperature (**Table 2**).

| Sample | Methane flow (sccm) | Hydrogen flow (sccm) | Pressure (Pa) | Temperature (°C) |
|---|---|---|---|---|
| 1 | 5 | 20 | 15 | 970 |
| 2 | 5 | 20 | 15 | 990 |
| 3 | 5 | 20 | 15 | 1030 |
| 4 | 5 | 20 | 15 | 1070 |

**Table 2.** (a) Graph image exhibiting the various steps of the growth process and (b) growth conditions of the different samples.

## 2.4. Strain control via the $H_2$ flow

To study the effect of hydrogen in the formation of ripples in the graphene surface, we have performed growths where only the flow of hydrogen is varying. The rest of the parameters are stable. Growth temperature is always 1040°C and the growth time is set in 20 min. The flow of methane is 5 sccm. We performed growth from 10 to 35 sccm $H_2$ (**Table 3**). The growth time was always 20 min. After that time, the furnace was opened and cooling to 500°C took about 10 s.

| Sample | Hydrogen flow (sccm) | Ripples density (number/μm) | 2D FWHM ($cm^{-1}$) | 2D position ($cm^{-1}$) | Strain ε (%) |
|---|---|---|---|---|---|
| A | 15 | 2.6 | 32.6 | 2719 | −0.002 |
| B | 20 | 3.6 | 26.6 | 2701.6 | −0.0011 |
| C | 25 | 3.8 | 24.75 | 2694.75 | −7.3E-4 |
| D | 30 | 4.3 | 30.4 | 2680.5 | −2.6E-5 |
| E | 35 | 4.3 | 30.75 | 2696 | −8.4E-4 |

**Table 3.** Experimental data of the ripples density and the 2D peak characteristics (position and FWHM). The strain is calculated through the 2D peak shift.

# 3. Results and discussion

## 3.1. Copper oxide reduction

During the hydrogen plasma treatment the hydrogen radicals react with the copper oxide reducing it to metallic copper [23]. We use optical emission spectroscopy to determine and

evaluate the reduction of the copper surface. The outcoming light from the discharge was collected by a spectrophotometer (Stellarnet EPP2000C), which operated in the range 300–850 nm. The evolution of the OH radical integral spectral intensity in the spectral range of 305–330 nm is a sufficient tool to evaluate the removal of the oxide [42]. Results show that the intensity of the peaks corresponding to OH radicals decrease after 5 min of plasma treatment. In particular, the first peak at 305 nm decreases from 22.6 to 5.9 a.u., as we can see in **Figure 4**. The reduction in the OH concentration reveals the reduction of the oxygen radicals (as a result of the oxide reduction). Nevertheless, as the copper oxide cannot be completely removed, the peak does not decrease more with further treatment [43]. **Figure 5(a)** shows the copper foil used as a substrate before (up and down sample) and after (medium sample) the hydrogen etching and the graphene growth. Graphene protects copper from oxidation which explains that even after the passage of days the reflected colour of the substrate does not change [44]. Copper foil before etching appears with a higher pitch of red because of the copper oxide layer on the top. After the treatment it appears brighter and large crystalline domains can be distinguished at naked eyes. This process is much more time sufficient, compared to the usual pre-annealing required for the Cu substrates taking up to several hours [32]. As an additional tool to characterize the copper surface, we used electron backscattered diffraction (EBSD). It
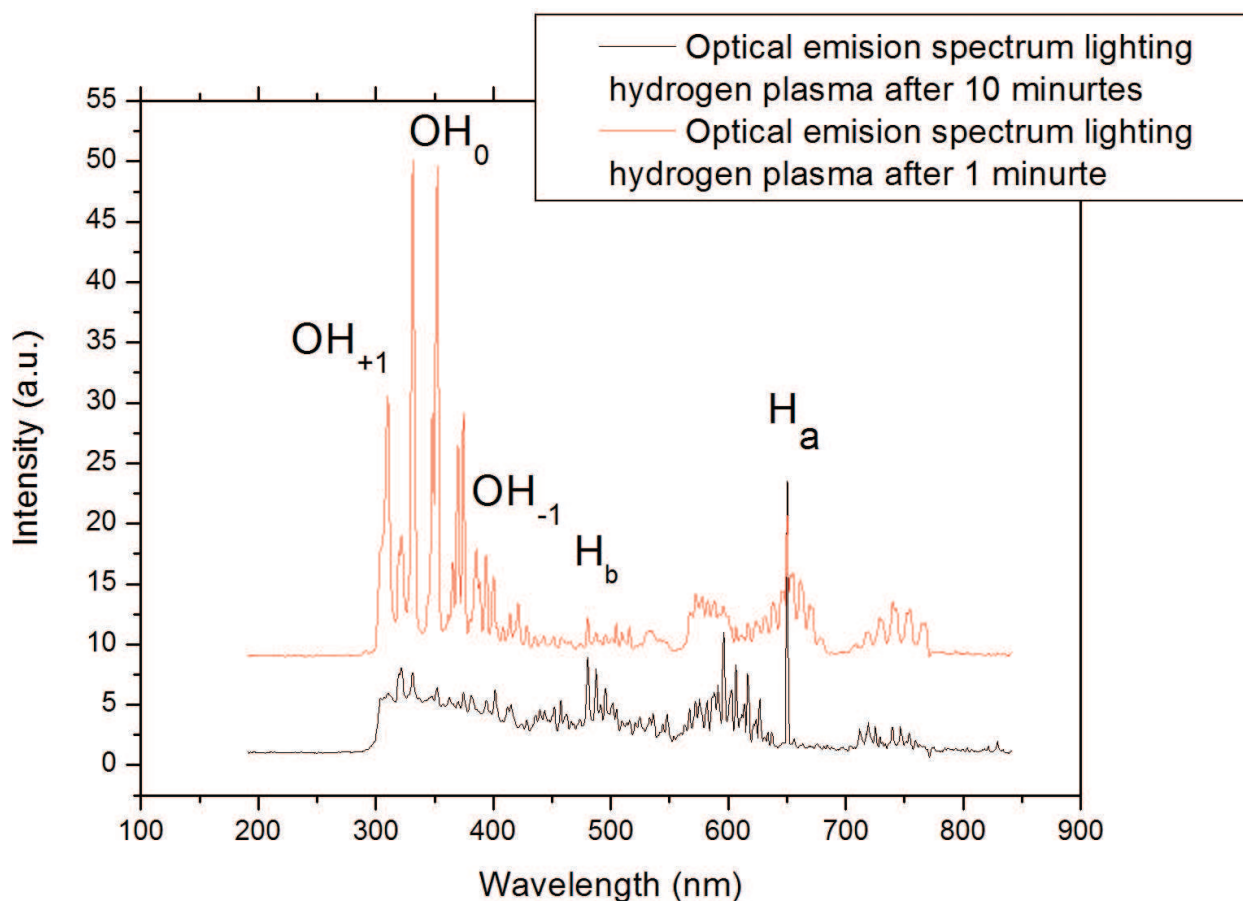


**Figure 4.** Optical emission spectroscopy of hydrogen plasma during reduction of copper: after 1 min (red line) and after 5 min (black line). The reduction of the OH radical peak intensity in the spectral range of 305–330 nm reveals the removal of the oxide layer.

**Figure 5.** (a) Polycrystalline copper foil before (up piece) and after (down piece) the hydrogen etching. The difference in the surface colour indicates the deoxidation of it. The red line indicates 4 cm. EBSD maps of (b) the as-received polycrystalline copper foil (scale bar 50 μm), (c) the foil after plasma annealing and 20 min graphene growth at 1040°C (scale bar 100 μm), and (d) the foil after plasma annealing and 50 min graphene growth (scale bar 200 μm).

is a large area imaging method which detects the different index copper facets. Here, EBSD is used in order to demonstrate the growth of the copper grains after the $H_2$ plasma and the growth process, with respect to the as-received copper foil. In **Figure 5**, we provide the EBSD mapping of untreated polycrystalline copper foil of 75 μm (**Figure 5(b)**), copper foil after 20 min growth (**Figure 5(c)**) and copper foil after 40 min growth (**Figure 5(d)**). As we see, the grains of the untreated copper have various sizes with most of them not overcoming ~30 μm². The boundaries between the grains are randomly oriented. During the heating and the growth the necessary energy is provided to the grains in order to increase in size. In our experiments, the heating is taking place under no presence of gas, in very high vacuum, and in the order of $10^{-4}$ Pa. The growth is taking place under the presence of hydrogen and methane, in a pressure

of ~20 Pa and in a temperature of ~1040°C. As we see in **Figure 5(c)** and **(d)**, with the longer growth, the grains grow larger. We see gains of sizes up to ~2000 $\mu m^2$ for the longer growth. The edges between the grains now are much straighter. These factors affect the quality of the grown graphene later. Graphene needs smooth and large grains to grow over. Usually, the boundaries are defect sites for the graphene, so the less possible boundaries mean the less possible defects.

### 3.2. Lobe's length and nucleation density of graphene bi-dimensional islands

Graphene crystals are grown forming planar dendritic geometries. The carbon species are being attached in the border of the islands. Varying the pressure results in formation of different graphene, considering both the size and the nucleation density of the domains. The nucleation density varies 8, 12, 37, 5 nuclei/10.000 $\mu m^2$, respectively, for 12.5, 15, 17.5 and 20 Pa. The different shapes of the domains that can be seen in **Figure 2a** are a result of the different copper orientation. As it has been explained [45] domains with four cusps grow over Cu (221) and domains with six cusps over Cu (310). The Raman spectra in the inset of **Figure 2b** ensures us about the single-layer nature of the graphene film. We can also observe some second-layer nucleation in some spots, below the first layer [46, 47]. We are interested in growing graphene with the lowest nucleation density possible, in order to decrease the amount of grain boundaries in the film, which usually introduce defects. For this reason, samples grown under 12.5 and 20 Pa are more adequate. We use a residual gas analyser to record the methane and hydrogen pressure during the growth. The $\delta P^H/\delta P^{CH4}$ ratio increases exponentially with the increase of the total pressure. This is probably due to the insufficiency of the turbomolecular pump to evacuate the low-mass atomic hydrogen. This results in higher concentration of hydrogen in the chamber.

Making some calculations, we observe that if the surface coverage is normalized with the quadratic lobe's length , we can extract the linear dependence between it and the nucleation density. In **Figure 6(a)**, we see the agreement between our experimental data and this model.

$$\frac{C}{L^2} = \frac{3\sqrt{3}}{2} n \qquad (2)$$

The value of the slope, $b = 1.5 \times 10^{-4}$, of the fitted line in **Figure 6(a)** is the constant of the surface growth rate, $dS/dt$ as a function of the lobes growth rate $dL/dt$.

In **Figure 6b–d**, we present the histograms of the results of the lobe's length size distribution measurements (independently of the copper facet) for the growth processes taking place at 12.5, 17.5 and 20 Pa. The two-peak distribution in histogram of **Figure 6d** is a result of the different growth velocity for the orientations of graphene cusps grown on the (310) copper crystalline facet. At 15 Pa, we have formation of a continuous layer, therefore we cannot estimate the size of the single domains.

### 3.3. Nucleation density and copper facet

From the SEM figures, we also observe a relation between the nucleation density and the copper orientation. Similar observations have been reported elsewhere [48]. According to the
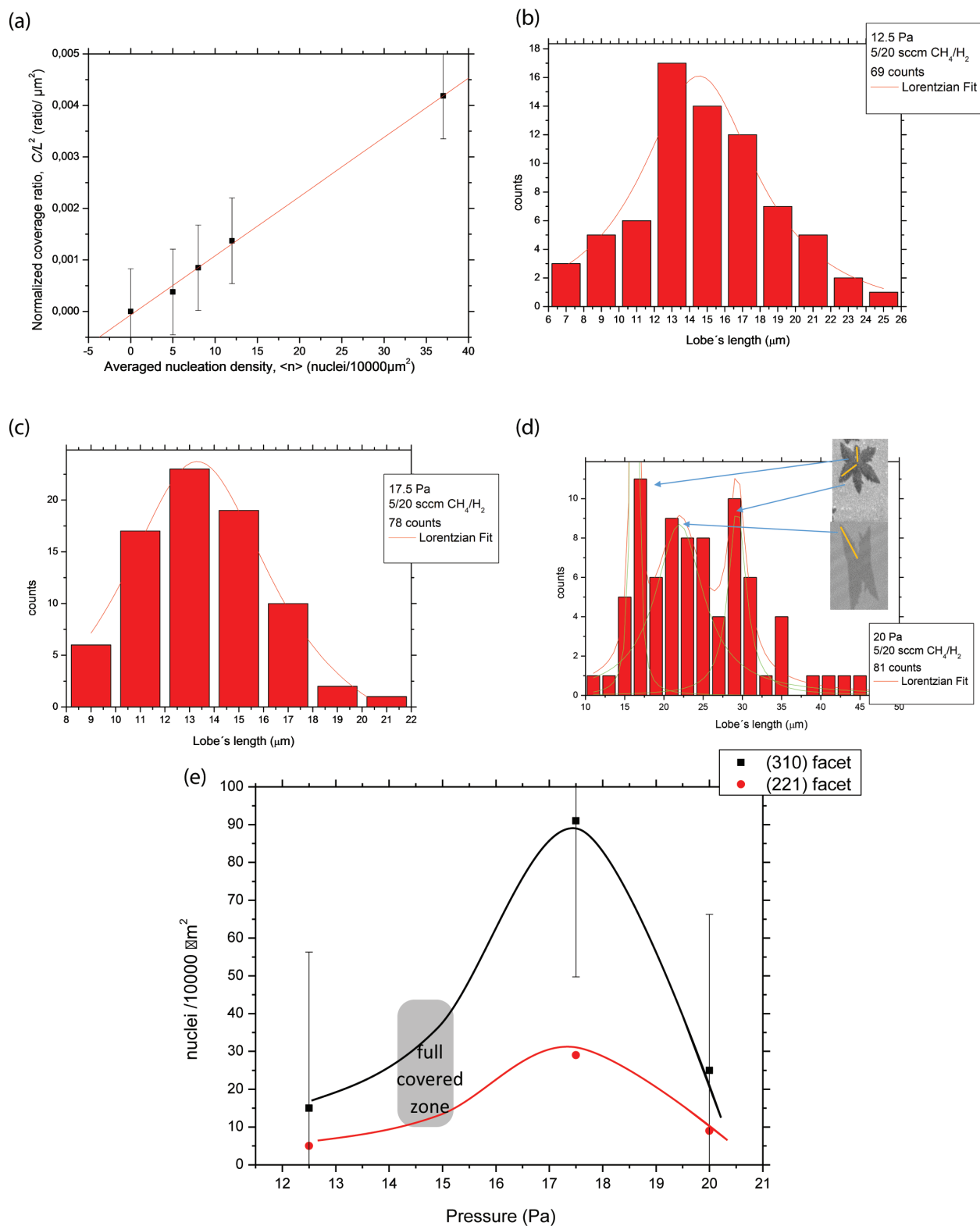
**Figure 6.** (a) Diagram demonstrating the linear dependence between the $C/L^2$ and the nucleation density. (b) Histogram of the lobe's length distribution measurements for the growth taking place in 12.5 Pa total pressure (c) and in 17.5 Pa. The tree peaks here is a result of the anisotropic growth of the lobe's in the (310) facet as well as the lobe's length in the (221) facet. (d) Same for 20 Pa total pressure. (e) Diagram presenting the variation in the nucleation density for each pressure and in relation to the copper facet. The copper facet (310) favours the nucleation.

shape of the graphene domains, in our samples, we observe nucleation over the copper facets (221) and (310). We observe that in all pressures, nucleation density is higher in the (310) facet. The results are demonstrated in **Figure 6e**. Thus, we can conclude that the facet (221) is more suitable for the growth of films with fewer boundaries. This is interesting to know as it establishes the possibility of growing graphene in single crystallinity copper surfaces.

### 3.4. Graphene coverage

Using the Image J software, we can know the percent surface coverage with graphene. We see that for the lowest nucleation, in 12.5 and 20 Pa, the coverage is lower that for the higher ones (**Figure 7**). The highest coverage appears in 15 Pa growth pressure. We observe that coverage plot follows a similar fluctuation as the nucleation density plot. On the right axis, we presented the $<P_{H2}>/<P_{CH4}>$ ratio of the average relative pressure values as a function of time, for the different total pressures, which follow a similar fluctuation as well, revealing a connection between the two. From the above, we underline the critical role of hydrogen. When its concentration is not sufficient, it cannot catalyze the graphene growth through the formation of active surface-bound carbon species $(C_yH_x)$s. When the concentration is too high, the etching effect is reinforced. Graphene nucleation, the growth rate and the termination size of grains are affected by competition of these two processes.
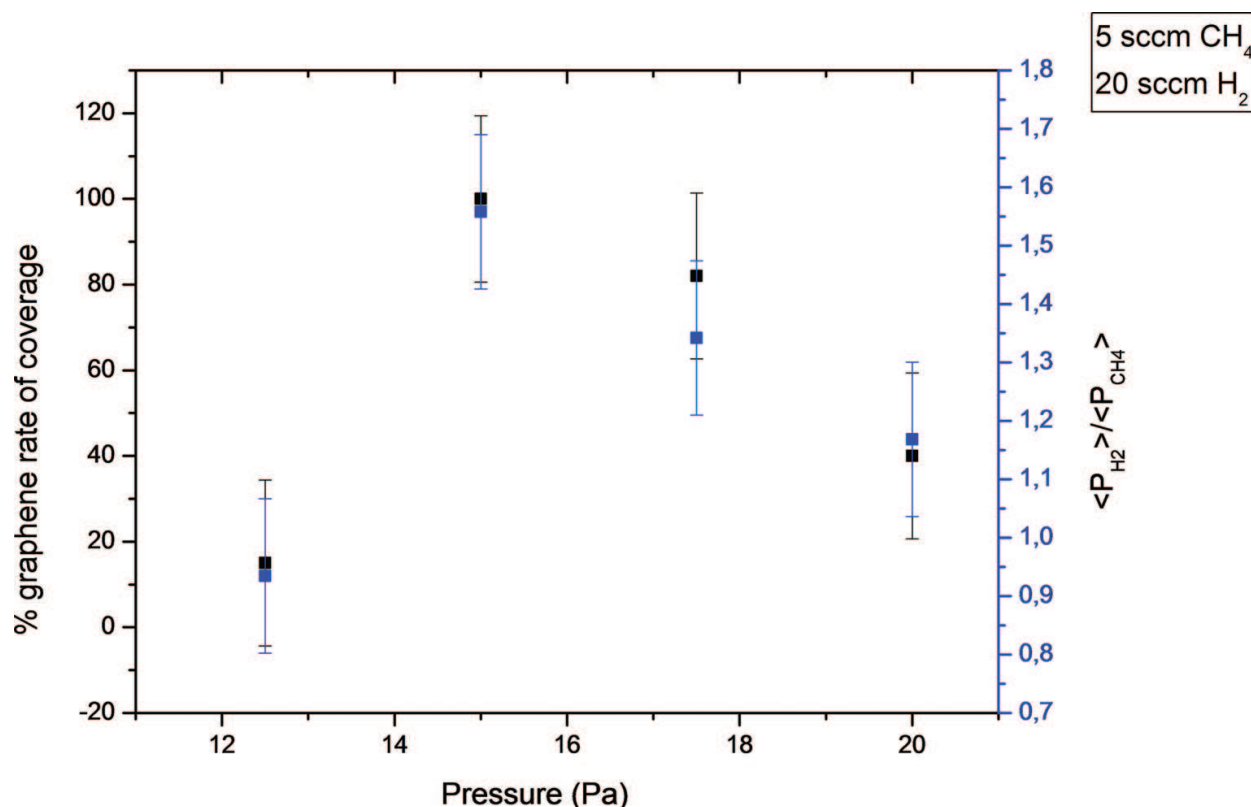


**Figure 7.** On the left Y axis we see thegraphene percent coverage of the surface as a function of the total pressure. On the right $Y$ axis we see the $<P_{H2}>/<P_{CH4}>$ ratio of the average relative pressure values as a function of time, for the different total pressures. The match in the variation of the values between the two graphs is evidence of the importance of hydrogen in the graphene growth.

### 3.5. Effect of the growing time

When we study the effect of growth time in the formation of graphene film, we can observe clearly the etching effect (**Figure 8**). We obtain a continuous film in 20 min. If we prolong the growth time, we observed the etching of the film and its damage as a result of the high hydrogen concentration in the chamber. To overcome this problem, techniques have been proposed which involve performing a two-step growth [14]. In the first step, a lower flow of methane is introduced in order to achieve low nucleation. In the second step, the methane flow and pressure increase in order to rapidly fill the gaps in the surface of the film.

### 3.6. Growth of graphene on large copper surface

We perform growth in larger copper pieces, 12 cm$^2$ with respect to 4 cm$^2$ that were used before. We do an extensive Raman analysis to study if graphene of same quality grows in the whole surface. The results indicate that single-layer graphene grows in the whole area, from the centre up to the edges. The spectra are obtained with a green laser. The G position appears at $1578 \pm 3$ cm$^{-1}$ and the 2D at 2671 cm$^{-1}$, confirming the single-layer nature of the film [49]. The $I_G/I_{2D}$ ratio is $0.27 \pm 0.03$ with a FWHM of 30 cm$^{-1}$. All data are presented in **Figure 9a**. Graphene of same quality is grown in the back side of the foil (**Figure 9b**). Then, the graphene is transferred onto different substrates, quartz and SiO$_2$, to study possible effects. The transfer is made by electrochemical delamination of the graphene [32]. By using this method, we avoid introducing any impurities from the metal etchant. G and 2D peak appear shifted by very few cm$^{-1}$. Such shifts can be due to edges, dislocations, cracks or vacancies in the sample that cause the so-called self-doping of the graphene [50].

### 3.7. Temperature effect

We are interested to study how the growth temperature can affect the nuclei formation and growth velocity of graphene. In addition, we study the formation of ripples in the graphene layer. The ability to control the formation of such ripples is of high interest if we want to obtain graphene films with enhanced mobility properties [37].
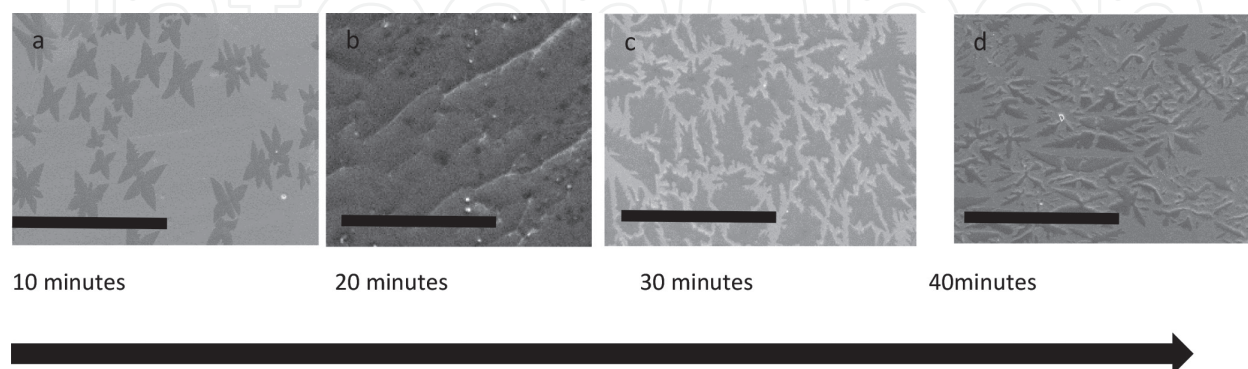


**Figure 8.** Variation of growth time. (a) At 10 min growth, 20 μm lobe's length crystals are obtained. (b) At 20 min growth, the film appears continuous. (c) At 30 min growth, the film appears partially damaged. (d) At 40 min growth, most of the graphene have been etched away from the catalyst substrate. The scale bar is always 50 μm.
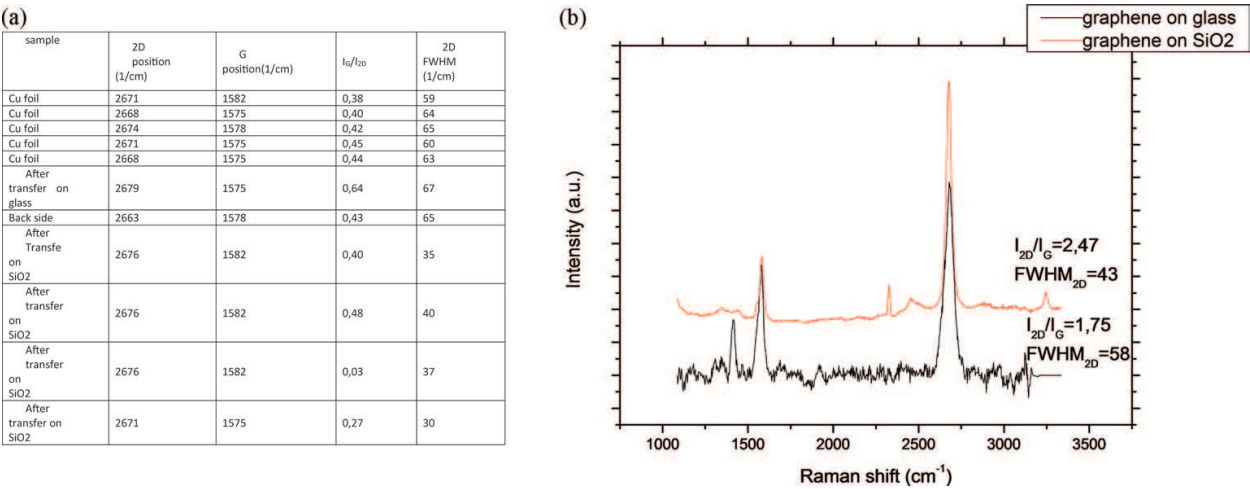
**Figure 9.** (a) Table presenting the Raman spectroscopy results. (b) Raman spectra after the transfer of the graphene film to glass (with thermally grown quartz on top, black line) and on $SiO_2$ (red line).

Considering the application of the hydrogen plasma, its efficiency in removing the copper oxide layer has been discussed in previous works of the authors [40] . In the same work, we provided back scattered electron microscopy figures where the evolution of the copper domains is shown. During the heating, the copper grains grow up, forming domains with size up to $10^4$ $\mu m^2$.

In **Figure 10**, we present the various scanning electron microscopy (SEM) images of graphene grown in different temperatures. **Figure 10a** corresponds to growth taking place at 970, (b) 990, (c) 1030°C and (d) 1070°C. We observe that nucleation of the graphene only occurs in the initial instants. This explains the high homogeneity in the graphene domains' size. In addition, higher temperatures lead to lower nucleation density and higher growth rates. No second layer nucleation below the first layer is observed in any of the figures.

In these figures, with the exception of **Figure 10d**, the domains do not reach the coalescence phase. Further growth times should be required to obtain a continuous graphene layer. Before, we have studied in depth the growth mechanisms of such continuous layers. We underline the dual role of the hydrogen in this process. Control of the growth is also performed through the growth pressure and its influence on the residence time of the carbon atoms in the surface. Careful selection of the above two parameters resulted in the formation of large continuous layers. Further extension of the growth time resulted in the anisotropic etching of the graphene.

Here we focus in the temperature effect and we study the kinetics of the graphene growth based on it. The study of the SEM figures provides information considering the nucleation density of the graphene crystals, growth velocity and surface coverage. Kinetics of two-dimensional graphene nucleation over copper has been studied both theoretically and experimentally by Kim et al. [51] before. When methane reaches the copper surface, it breaks down. The concentration of carbon active species increases until it reaches a critical supersaturation level. Nucleation starts upon this point. Nucleation and growth of the supersaturated nuclei deplete the adsorbed carbon species surrounding them and the nucleation rate becomes negligible. The growth of the nuclei continues until supersaturated amount of surface carbon species is consumed and equilibrium
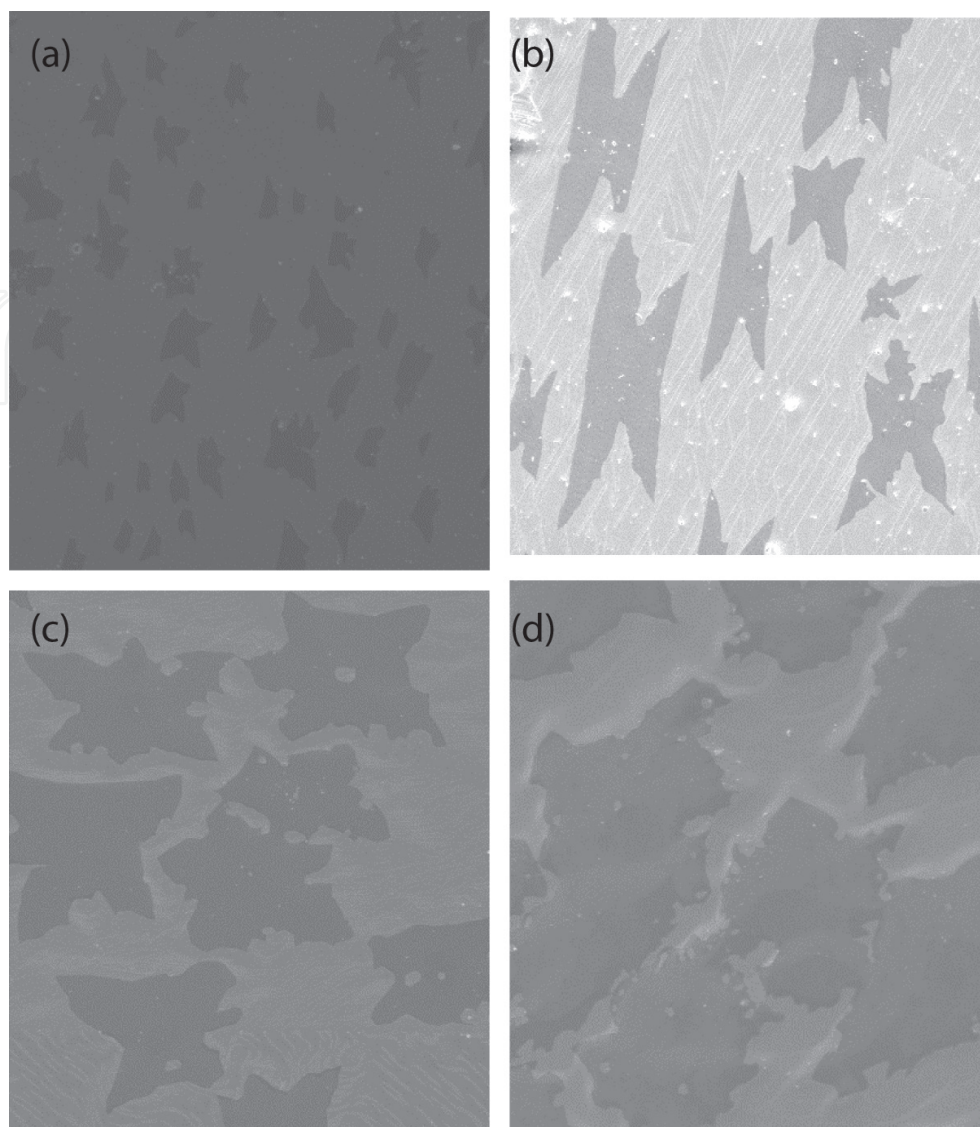
**Figure 10.** SEM images of graphene domains grown in different temperatures: (a) at 970, (b) 990, (c) 1030 and (d) 1070°C. The $X$ axis is always 100 μm.

between graphene, surface carbon and $CH_4/H_2$ is reached. Depending on the amount of available carbon, graphene domains will either coalesce to form a continuous layer or stop growing to reach a saturated, final incomplete coverage [52].

To understand the kinetics of the existing nucleation model, we study the nucleation density and growth rate with respect to the growth temperature. In **Figure 11a**, we show the Arrhenius plot of the temperature-dependent density of graphene nuclei. According to Robinson model [53], there are two nucleation regimes which are a result of the competition between the processes of adatom capture, surface diffusion and re-evapouration. In the high temperature regime ($T > 870$°C), the desorption of the carbon adatoms is significant compared to their mobility, so their lifetime and nucleation rate is desorption-controlled. The decrease in the nucleation density for increasing temperatures is explained due to the increase of the desorption rate, reducing the probability of further nucleation, as discussed by Kim et al. [51].
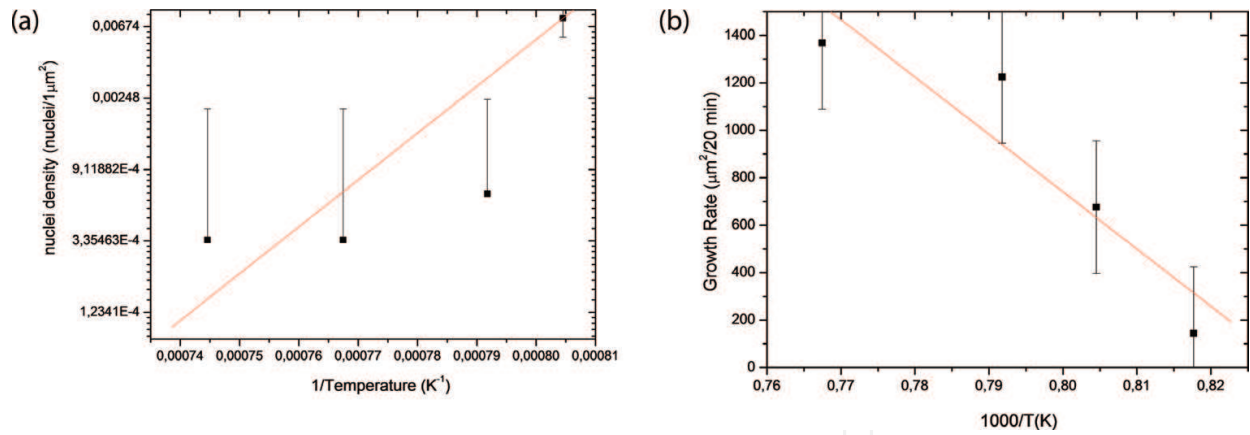
**Figure 11.** (a) Analysis of graphene nucleation behaviour. Natural logarithm of density of graphene nuclei versus $1/T$ from SEM analysis. (b) Linear plot of the graphene nucleus growth rate versus $1000/T$.

In **Figure 11b**, we observe how the growth rate increases with the increase of the growth temperature. In this plot, we assume that the growth is linear for the growth time. Higher growth rates occur thanks to the lower nuclei density. Previous studies [51] have shown no significant differences of the growth rates on three main crystalline orientations [Cu(111), Cu(100) and Cu(103)] of the polycrystalline Cu.

To calculate the activation energy, we will apply the kinetic model proposed by Xing et al. [54]. According to this model, growth rate is proportional to the uncovered copper surface.

$$\frac{d\text{coverage}}{dt} = a\big(1 - \text{coverage}\big) \tag{3}$$

According to the above equation, the rate is the highest in the initial moments and decreases during the graphene growth. By integrating it, we derive the coverage equation coverage $= - e^{at} + 1$ where $t$ is the time and $a$ is a constant defined by the growth temperature. As seen in **Figure 12b**, coverage increases with the increase in temperature, result which can be explained taking into account the previous observations considering the nucleation density and growth rate behaviour. On the same time, $a$ increases with the temperature as well. To calculate the activation energy $E$ of the graphene growth, we use the Arrhenius equation $a \sim e^{-E/kT}$, where $k$ is the the Boltzmann's constant and $T$ is the absolute temperature. From the Arrhenius plot of **Figure 12a**, we can extract the activation energy from the slope of the linear fit. The activation energy is calculated to be 3.01 eV. In previous studies, a wide range of activation energies (1–3) have been proposed for graphene growth over copper. The energy barrier depends on the growth temperature and on the dominant nucleation mechanism. In lower temperatures, the adsorption energies of carbon monomers depend on the crystalline orientation of copper [55]. In higher temperatures, where desorption is the principle responsible nucleation mechanism, the differences in activations energies are minimal with respect to the copper orientation, both for low and atmospheric pressure CVD [11].
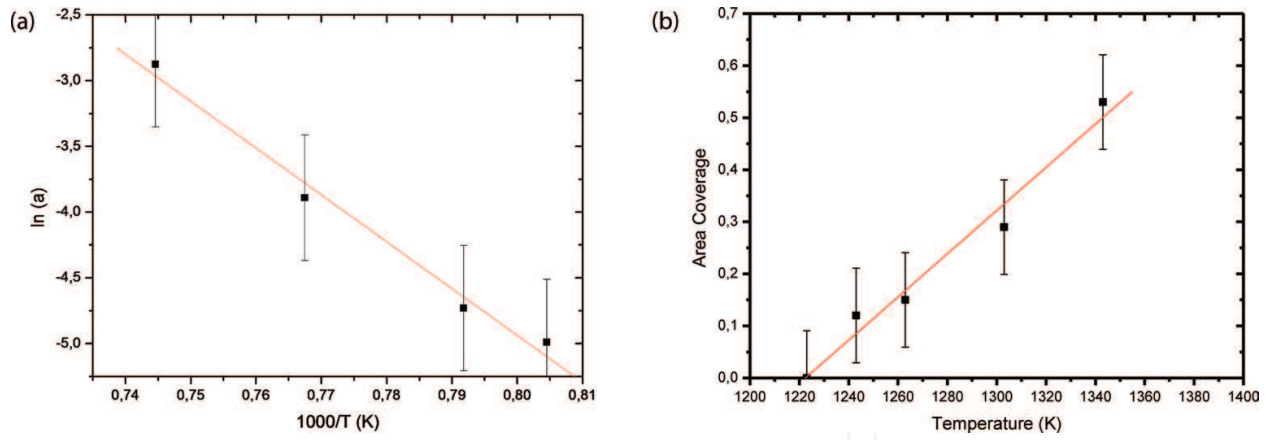
**Figure 12.** (a) Arrhenius plot of the ln (a) as a function of 1000/T. From the slope of the linear fitting we obtain the activation energy. (b) Graphene coverage on Cu as a function of different growth temperatures.

### 3.8. Strain control via the H$_2$ flow

By the SEM images, we could determine the density of the ripples in each sample. **Figure 13** shows the SEM images for the different hydrogen flows in the studied range.

**Figure 14a** provides the Raman spectrum corresponding to samples grown at different hydrogen flows. The copper photoluminescence background has been removed from all the spectra. In previous works, the copper luminescence has been attributed to the different quenching effect of the deposited graphene owing to probably irregular thickness distribution. Another explanation can be the quenching effect of graphene as a function of distance between Cu surface and graphene. The suspended graphene can result from the ripple's formation in the copper surface during the cooling step [37]. In **Figure 14b**, we can see an enlarged image of the above spectra where the shift in the 2D peak becomes evidenced by the evolution of the hydrogen flow.

The absence of a D peak in the spectra presented in **Figure 14a** proves the highly crystalline nature and the absence of defects in the graphene films. The ration $I_D/I_G$ is proportional to the mean distance between two defect points in a graphene film. The absence of the D peak corresponds to pristine graphene [56]. A small D peak can be distinguished in the spectra corresponding to graphene growth under the higher hydrogen flow rate (35 sccm) probably owing to the hydrogen etching on the graphene surface. The defects concentration of the graphene surface can be obtained by Eq. (4) [57]

$$n_D(\text{cm}^{-2}) = \frac{10^{14}}{\pi^2 \left[ C_A \left( r_A^2 - r_S^2 \right) + C_S \, r_S^2 \right]} \frac{I_D}{I_G} \tag{4}$$

$$n_D = 1.02 \times 10^{11} \text{ cm}^{-2} \tag{5}$$

Where $r_A$ and $r_S$ are the radius of two circular areas measured from the defect site. The first length, $r_S$, is the radius of the structurally disordered area around the defect. $r_A$ defines the disk where the D peak scattering takes place and it defines the activated area. $C_A$ depends only on the Raman mode, being roughly given by the ratio of the electron-phonon coupling
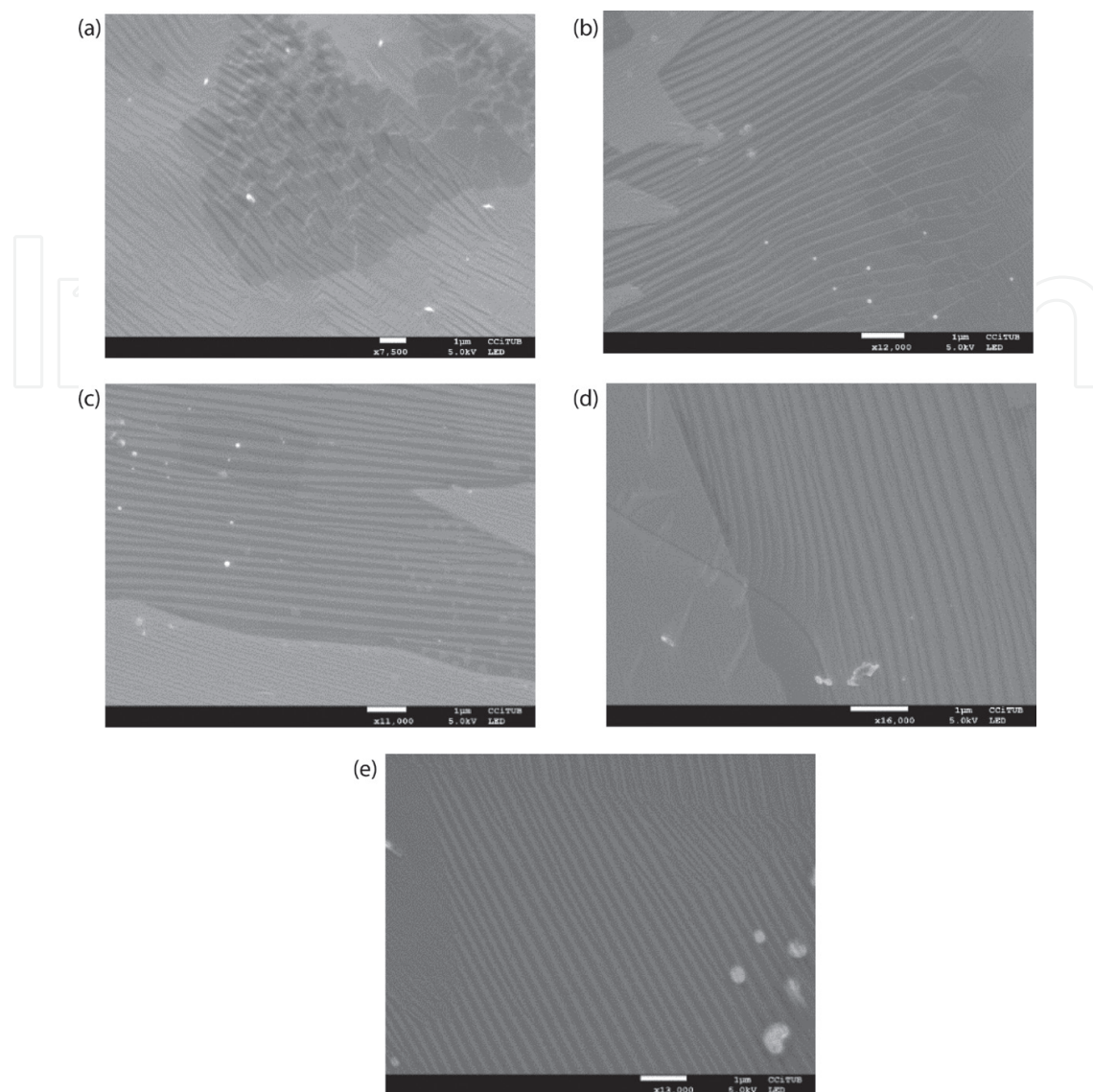
**Figure 13.** SEM images of graphene/copper surface: (a–e) graphene films growth at different hydrogen flows, resulting in an increase in the ripple's density. (a) 15, (b) 20, (c) 25, (d) 30 and (e) 35 sccm hydrogen flow. Scale bar is always 1 μm.
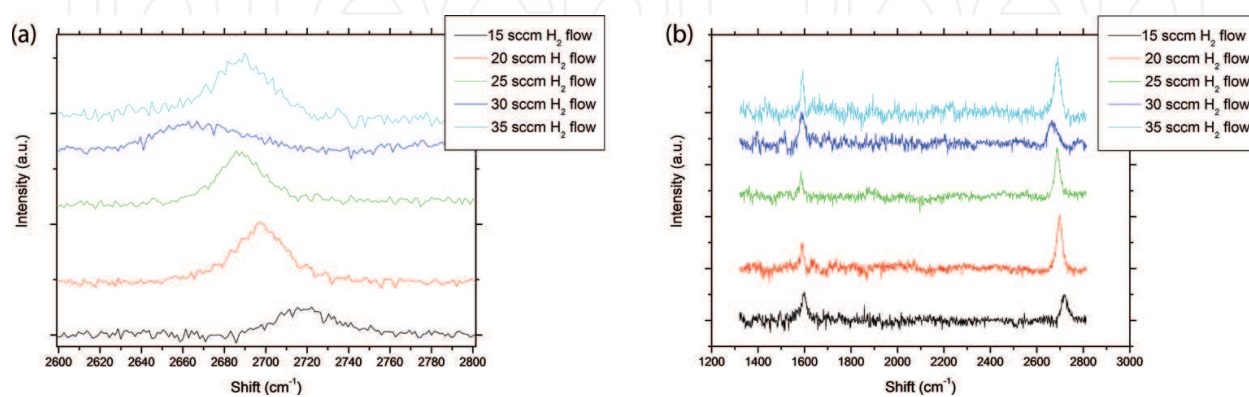


**Figure 14.** (a) Raman spectra of the different samples grown at several hydrogen flow rates. (b) Enlarged figure of the 2D peak of the same samples.

between the two phonons considered. $C_{S,x}$ represents the Raman cross section of $I(x)/I(G)$ associated with the distortion of the crystal lattice after defect introduction per unit of damaged area. The following parameters were reported for intensity measured as height: $r_A \sim 3$ nm, $r_S \sim 1$ nm, $C_A = 4.2$, $C_S = 0.87$ [57]. For samples grown at lower hydrogen flow rate, the presence of defects from Raman analysis is negligible.

In previous works [58], the formation of ripples in graphene during CVD growth has been studied. During CVD growth, graphene tends to replicate the morphology of the substrate. When graphene is grown over copper foil, the formation of these ripples is a common phenomenon. When the copper foil is exposed at the same heating and cooling process (as CVD graphene growth) but in the absence of any hydrocarbon, no ripples are formed and the formation of dendrite-like structures or 'snowflakes' is observed. Therefore, the presence of hydrocarbon seems a necessary condition for the formation of ripples.

One possible mechanism describing the ripple's formation is the following. At high temperatures, above 1000°C, a massive near-surface movement of the copper atoms takes place underneath the growing graphene. This gives rise to the surface reconstruction and to the formation of nano-ripples. While cooling down to room temperature, the copper substrate contracts, whereas the graphene which is on top tries to expand according to its negative thermal expansion coefficient [59]. In the areas where graphene is pinned to the copper, it is displayed to a strong compressive stress, whereas in the areas where the graphene is suspended above the nano-ripples it is allowed to relax some amount of the compressive strain through out-of-plane deformation (rippling) [60–61].

In the present work, when we measure the ripples in the samples corresponding at different hydrogen flows, a sigmoid increase of the density of ripples at higher hydrogen flows takes place (**Figure 15**). More specifically, the ripple density increases from 2.6 to 4.3 ripples/μm while the hydrogen flow increases from 15 to 30 sccm (with a step of 5 sccm). Finally, at 35 sccm of hydrogen flow the ripple density is 4.3 ripples/μm as well.

In all above described experiments, the methane flow was kept constant; therefore, the variation of the hydrogen flow is the factor that apparently affects the density of the formed ripples. **Figure 16** shows the Raman measurements of the different hydrogen flows. In **Figure 16a**, we see the full width half maximum (FWHM) of the 2D peak versus the hydrogen flow. Despite some extreme values, mainly in the samples grown at 25 and 30 sccm of hydrogen flow, the majority of the spectra presents an FWHM close to the value of 28 cm⁻¹, which is the reference value of the 2D peak FWHM for single-layer graphene [62 ]. Narrower 2D bands are correlated with flat and undoped regions on the Cu (100) and (110) surfaces. The generally compressed (0.3% of strain) and n-doped (Fermi level shift of 250 meV) graphene on Cu (111) shows the 2D band FWHM minimum of 20 cm⁻¹. In contrast, graphene grown on Cu foil under the same conditions reflects the heterogeneity of the polycrystalline surface and its 2D band is accordingly broader with FWHM > 24 cm⁻¹ [63]. The authors have previously studied the polycrystalline nature of the copper surface by electron backscatter diffraction (EBSD) mapping. After the heating up to 1040°C and posterior cooling, the domains increase significantly in size. According to these observations, graphene domains grow forming different morphologies which depend on the copper lattice orientation, in accordance to previous
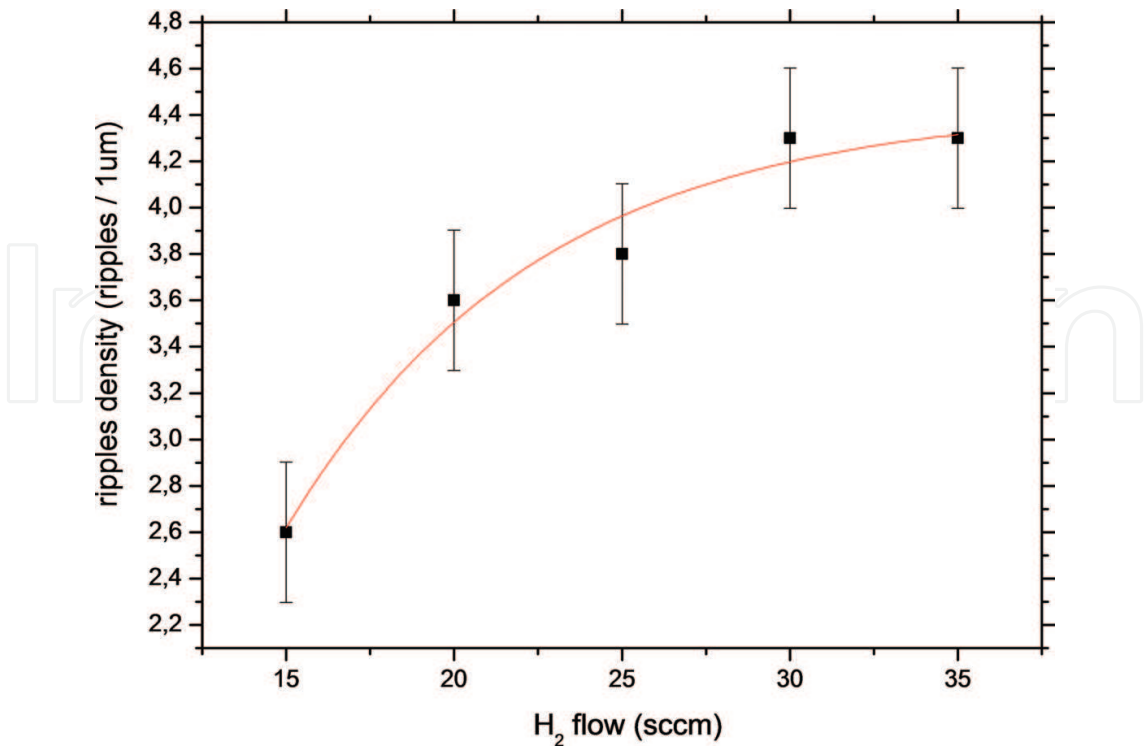
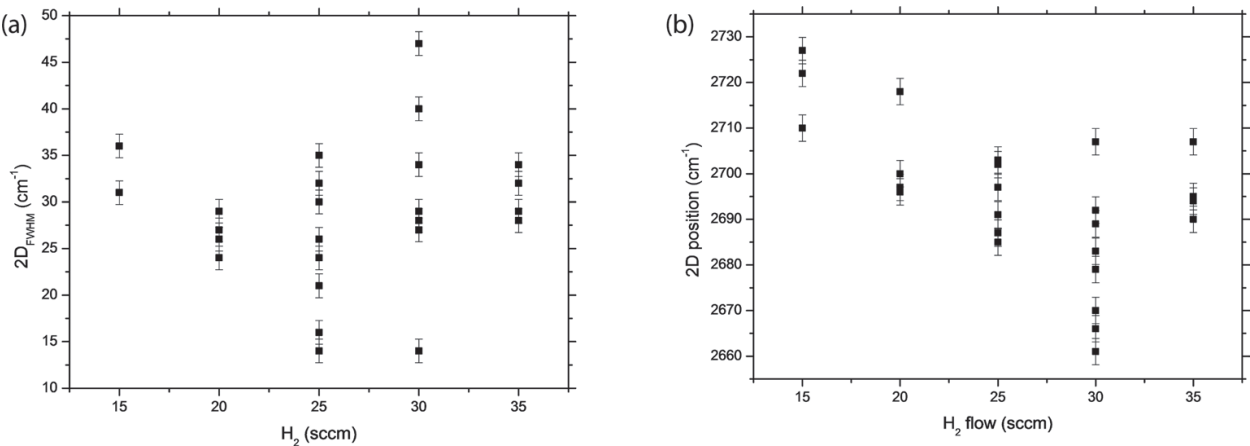**Figure 15.** Ripples density of graphene for various hydrogen flows.



**Figure 16.** (a) Plot of the 2D FWHM with respect to the different hydrogen flows. The blue line corresponds to the reference value of the 2D peak FWHM for single-layer graphene, (b) plot of the 2D position with respect to the different hydrogen flows. The blue line at 2680 cm$^{-1}$ corresponds to the position of relaxed graphene.

theoretic and experimental results[45]. In concrete, we have observed how graphene domains with a four-lobe morphology grow over the Cu (100) plane, while graphene domains with a butterfly-like morphology grow over the Cu (221) plane.

By the shift in the 2D peak, we calculate the graphene strain. **Figure 16b** shows the position of the 2D peak versus the hydrogen flow. The position of the 2D peak shifts from 2719 to 2680 cm$^{-1}$ with the increase of the hydrogen flow from 15 to 30 sccm. The values presented in **Table 1** regarding the 2D FWHM and the 2D position for the different hydrogen flows are the average values resulting from those presented in the plots of **Figure 16a** and **b**.

The results reveal an average red-shift of the 2D peak following the hydrogen flow increase. We have associated this shift with the strain introduced to the graphene as a result of the ripple's formation and the partial ablation of graphene. Such shifting of the 2D peak between suspended and supported graphene has been observed before [64]. Rao et al. have observed a shifting of the order of 10 cm$^{-1}$. In our case, we propose to explain the decrease of the compressive strain effect as the origin of this shift. As mentioned earlier, the graphene replicates the morphology of the copper substrate. In order to understand this phenomenon, we propose a mechanism based on thermal mobility of Cu adatoms. Surface adatoms can take energy from hydrogen bombardment, which facilitates their migration and ripple's formation.

Theory of thermal grooving was first developed by Mullins et al. [65]. In this work, surface migration is proposed as the most probable mechanism of groove formation. The origin of the grooves can be due to evapouration or due to surface diffusion of the copper adatoms. As temperature falls, surface diffusion is favoured thanks to its small activation energy, in compare to the enthalpy of evapouration. Although, in their model, Mullins et al. consider that the grooves are formed during the heating of the surface. As the development of the groove is proportional to $t^{1/4}$, where $t$ is the annealing time, they come in accordance with experimental results which indicate that the grooves did not develop more after some hours of annealing.

Today we know thank to *in situ* observations that the grooves, or ripples as we refer to in our text, develop during the cooling step. As observed by *in situ* scanning electron microscopy [66], ripples are formed in the copper surface during the cooling step, in concrete in the range between 600 and 700°C. Surface re-construction of the pre-melted copper occurs in this range of temperatures.

The model proposed by Mullins allows us to calculate the depth of the groove when we know the separation of two consecutive maxima.

$$\frac{s}{d} = \frac{4.73}{m} \qquad (6)$$

where $s$ is the separation between the two maxima, $d$ is the groove depth and $m = \tan b = 0.10$ ($b$ is the equilibrium angle).

As we know the separation of the two maxima from the SEM images (~0.5μm), we calculate the depth $d$ = ~10 nm. Values of this order are very similar to the ones observed by other authors [67].

The increase in the hydrogen bombardment increases the adatoms density and, therefore, the ripple's density. From molecular dynamic simulations that have been performed by Rosen et al. [68], it has been calculated that the positive energy transfer that can occur during the bombardment of metallic clusters by a gas. This energy can promote the diffusion of the metallic adatoms, promoting the formations of ripples. Graphene grows overlapping the copper ripples. The migration of the copper adatoms results in the formation of convex regions where copper is disordered. Ordered copper adatoms remain in the concave regions (**Figure 17a**) [69]. The ordered placement of the copper adatoms in these regions favours the matching with the graphene.
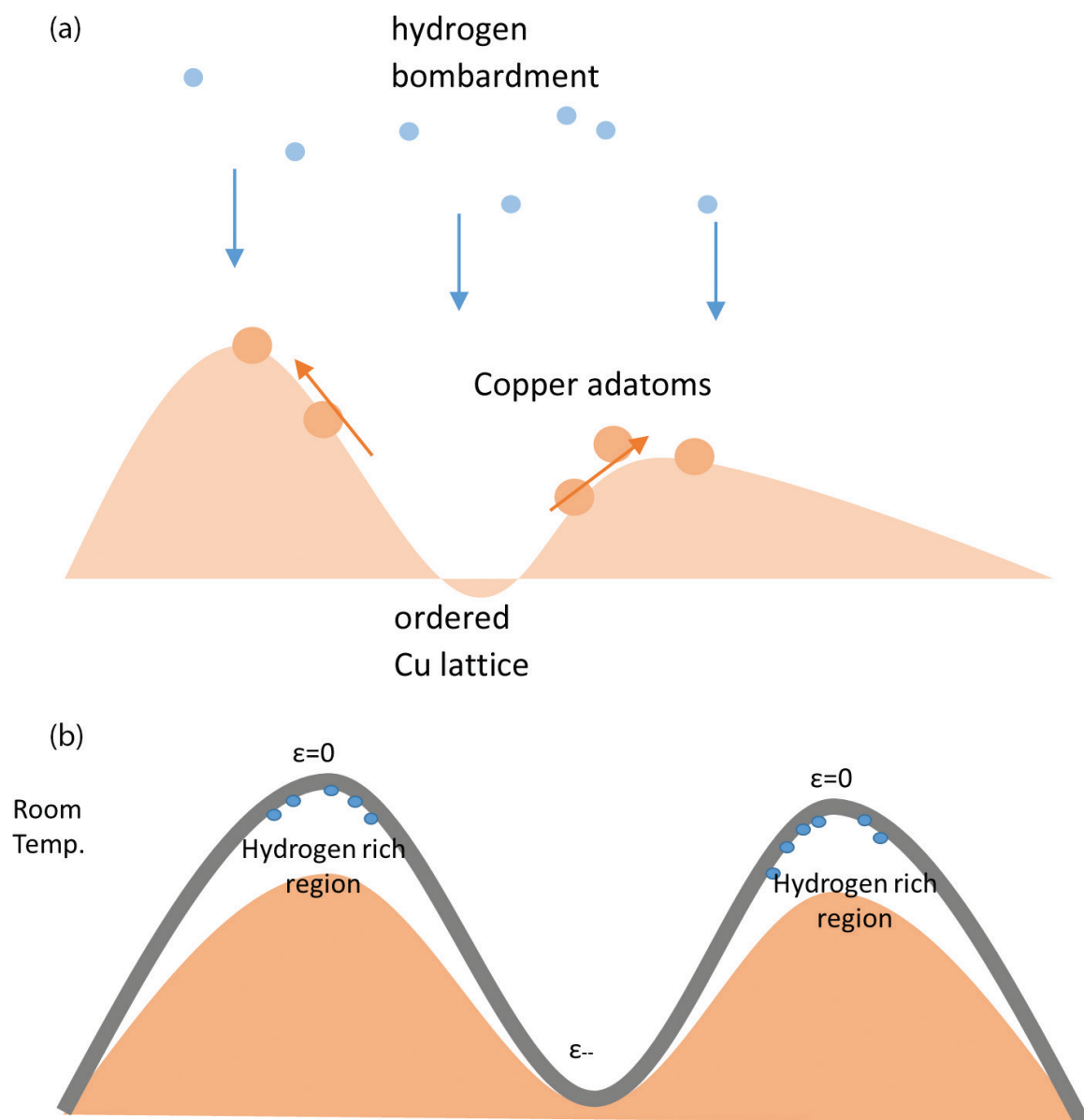
**Figure 17.** (a) Illustration of the ripple's formation as a result of the hydrogen bombardment. (b) Aspect of the graphene film after its ablation from the concave regions.

As explained above, while cooling, the copper foil contracts. This induces an increase in the compressive stress of the graphene in the concave region. In the convex region, the graphene detaches from the copper and remains suspended and relaxed. This detachment probably is the reason that graphene in the convex regions favours the hydrogen storage. As explained in previous works by experimental and density functional theory calculations [69], graphene chemisorption of atomic hydrogen is energetically favourable in the convex regions (**Figure 18b**). In that work, scanning tunnelling microscopy (STM) images have shown a large increase in corrugation due to the C–H bonds on the convex areas of the graphene surface after the exposure of pristine graphene to atomic hydrogen. DFT simulations have observed and resolved hydrogen dimers and tetramers on top of the carbon atoms, on distances that do not extend beyond 4 Å between them.
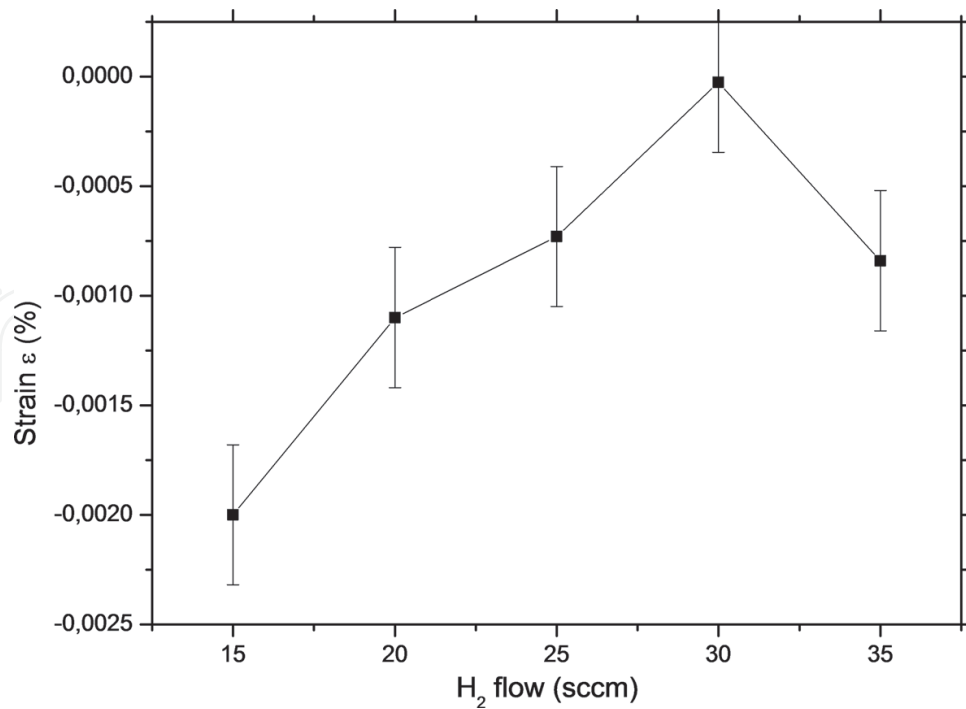
**Figure 18.** Calculated compressive strain (Eq. 7) of graphene layer for the different hydrogen flow rates from the 2D Raman peak shift.

According to Goler et al. [69] calculation and using 650°C (~930 K) as the approximate temperature of the hydrogen desorption from the puckered graphene, the only positions where hydrogen is stable at elevated temperatures, a desorption energy barrier of 1.4 eV is calculated. The hydrogen dimers are calculated to be as stable as molecular hydrogen. This is a result of the favourable hydrogen chemisorption on the convex areas, like we propose in the model of **Figure 5b**. In this case, the local curvature increases after the first H atom is adsorbed because the carbon atom protrudes out of the graphene plane. This effect induces adhesion of subsequent H atoms. In accordance with Goler et al., the adhesion of atomic hydrogen becomes thus barrierless.

In our work, we consider that the red-shift of the 2D peak is a result of the reduction/absence of the compressive strain with the increase in the hydrogen flow. With the increase in the ripples density, more regions where graphene is relaxed are contained in each spectrum, resulting in reinforcing of the red-shift of the 2D peak.

From the shift in the 2D peak, we can calculate the strain of the graphene. This is calculated by equation

$$\varepsilon = \frac{-\Delta u_{2D}}{2 u_{2D}^0 \gamma_D} \tag{7}$$

where $\varepsilon$ is the value of the strain, $\gamma_D$ = 3.55 is the Gruneisen parameter and $\Delta u_{2D}$ denotes the shift of the frequency of the 2D phonon mode with respect to $u_{2D}^0$ = 2680 cm$^{-1}$ (which is the position of the 2D peak for unstrained pristine graphene) [70]. The compressive strain is reduced with the increase of the hydrogen flow from $\varepsilon$ = −0.2% for 15 sccm of hydrogen to $\varepsilon$ = −0.026% for 30 sccm of hydrogen flow rate (**Figure 18**).

## 4. Conclusions

In the present chapter, we study the CVD growth of graphene over copper foils. We are interested in the effect of the growth parameters, gases mixtures, pressure, temperature in the graphene synthesis. The characterization of SEM images gives information about the effect of hydrogen in the process. The lower nucleation density results in formation of larger crystals but lower total coverage. Considering the coverage, the etching effect of hydrogen in the graphene film plays an important role. In addition, we underline the linear dependence between the $C/L^2$ and the nucleation density. We highlight the increase of hydrogen partial pressure under stable flow and the fact that the relative pressure $<P_{H2}>/<P_{CH4}>$ ratio diagram follows the same variation as the percent coverage diagram.

We study the kinetics, from a perspective of temperature dependence, of CVD-grown graphene in low pressure and over polycrystalline copper substrate. Growth temperature ranges between 970 and 1070°C. The growth takes place in a methane/hydrogen atmosphere. In all samples, high-quality, defect-free single-layer graphene is grown, as revealed by Raman spectroscopy. SEM images analysis provide information considering the nucleation density, in the range between 0.5 and 8 nuclei/1000 $\mu m^2$, and the growth rate, in the range between 150 and 1400 $\mu m^2$/20 min, of the graphene domains. Activation energy of 3.01 eV has been derived from the Arrhenius equation. Finally, we study the profile of the ripples formed in the graphene surface. Ripples of 0.2 $\mu m$ and 4 nm height are formed, introducing an intrinsic strain in the graphene. The geometry of the ripples is not affected by the growth temperature.

Through the control of the flow, the ripple density is regulated. An increase in the flow of hydrogen can reduce the compressive strain, as a result of the levitation of graphene from the copper substrate in the concave regions. However, the introduced hydrogen flow should be selected with care, as high flow rates can lead to anisotropic etching of the graphene film.

## Acknowledgements

## Author details

Stefanos Chaitoglou*, Enric Bertran and Jose Luis Andujar

*Address all correspondence to: schaitog@gmail.com

FEMAN Group, IN2UB, Department of Applied Physics, University of Barcelona, Barcelona, Catalonia, Spain

# References

[1]    Li X et al. Large-area synthesis of high-quality and uniform graphene films on copper foil. Science 2009;**324**:1312–4.

[2]    Bae S et al. Roll-to-roll production of 30-inch graphene films for transparent electrodes. Nat. Nanotechnol. 2010;**5**:574.

[3]    Han G H, Shin H-J, Kim E S, Chae S J, Choi J-Y and Lee Y H. Poly(ethylene co-vinyl acetate)-assisted one-step transfer of ultra large graphene. Nano 2011;**6**:59.

[4]    Miseikis V et al. Rapid CVD growth of millimetre-sized single crystal graphene using a cold-wall reactor. 2D Mater. 2010;**2**:014006.

[5]    Yazyev O V and Louie S G. Topological defects in graphene: dislocations and grain boundaries. Phys. Rev. B 2010;**81:**195420.

[6]    Li X F, Wang L L, Chen K Q and Luo Y. Effects of interface roughness on electronic transport properties of nanotube–molecule–nanotube junctions. J. Phys. Chem. C 2010;**115**:12616–24.

[7]    Kumar S B and Guo J. Strain-induced conductance modulation in graphene grain boundary. Nano Lett. 2012;**12**:1362.

[8]    Yazyev O V and Louie S G. Electronic transport in polycrystalline graphene. Nat. Mater. 2010;**9**:806–9.

[9]    Gran Table R, Shenoy V B and Ruoff R S. Anomalous strength characteristics of tilt grain boundaries in graphene. Science 2010;**330:**946–8.

[10]   Kim K, Artyukhov V I, Regan W, Liu Y, Crommie M F, Yakobson B I and Zettl A. Ripping graphene: preferred directions. Nano Lett. 2012;**12**:12293–7.

[11]   Vlassiouk I et al. Graphene nucleation density on copper: fundamental role of background pressure. J. Phys. Chem.C 2013;**117:**18919–26.

[12]   Li X, Magnuson C W, Venugopal A et al. Large-area graphene single crystals grown by low-pressure chemical vapour deposition of methane on copper. J. Am. Chem. Soc. 2011;**133**:2816–9 .

[13]   Bhaviripudi S, Jia X, Dresselhaus M S and Kong J. Role of kinetic factors in chemical vapour deposition synthesis of uniform large area graphene using copper catalyst. Nano Lett. 2010;**10**:4128–33.

[14]   Li X, Magnuson C W, Venugopal A. et al. Graphene films with large domain size by a two-step chemical vapour deposition process. Nano Lett. 2010;**10**:4328–34.

[15]   Wu B, Geng D, Xu Z, Guo Y, Huang L, Xue Y, Chen J, Yu G and Liu Y. Self-organized graphene crystal patterns. NPG Asia Mater. 2013;**5**:36.

[16]   Zhang Y, Li Z, Kim P, Zhang L and Zhou C. Anisotropic hydrogen etching of chemical vapour deposited graphene. ACS Nano 2011;**6:**126–32.

[17] Geng D,Wu B, Guo Y, Luo B, Xue Y, Chen J, Yu G and Liu Y. Controllable synthesis of submillimeter single-crystal monolayer graphene domains on copper foils by suppressing nucleation. J. Am. Chem. Soc. 2013;**135**:6431–4.

[18] Vlassiouk I, Regmi M, Fulvio P, Dai S, Datskos P, Eres G and Smirnov S. Role of hydrogen in chemical vapour deposition growth of large single-crystal graphene. ACS Nano 2011;**5:**6069–76.

[19] Zhang X, Ning J, Li X, Wang B, Hao L, Liang M, Jin M and Zhi L. Hydrogeninduced effects on the CVD growth of high-quality graphene structures. Nanoscale 2013;**5:**8363–6.

[20] Ma T, Ren W, Zhang X, Liu Z, Gao Y, Yin LC, Ma XL, Ding F and Cheng H M. Edge-controlled growth and kinetics of single crystal graphene domains by chemical vapour deposition. Proc. Natl Acad. Sci. USA 2013;**110**:20386–91.

[21] Mohsin A et al. Synthesis of millimeter-size hexagon-shaped graphene single crystals on resolidified copper. ACS Nano 2013;**7:**8924.

[22] Yan Z, Lin J, Peng Z, Sun Z, Zhu Y, Li L, Xiang C, Samuel E L, Kittrell C and Tour L M. Toward the synthesis of wafer-scale single crystal graphene on copper foils. ACS Nano 2012;**6:**9110–7.

[23] Wu Y A, Fan Y, Speller S, Creeth G L, Sadowski J T, He K, Robertson A W, Allen C S and Warner J H. Large single crystals of graphene on melted copper using chemical vapour deposition. ACS Nano 2012;**6:**5010–7.

[24] Geng D,Wu B, Guo Y, Huang L, Xue Y, Chen J, Yu G, Jiang L, Hu W and Liu Y. Uniform hexagonal graphene flakes and films grown on liquid copper surface. Proc. Natl Acad. Sci. USA 2012;**109:**7992–6.

[25] Wang H, Wang G, Bao P, Yang S, Zhu W, Xie X and Zhang W J. Controllable synthesis of submillimeter single-crystal monolayer graphene domains on copper foils by suppressing nucleation. J. Am. Chem. Soc. 2012;**134**:3627–30.

[26] Wu T, Ding G, Shen H, Wang H, Sun L, Jiang D, Xie X and Jiang M. Triggering the continuous growth of graphene toward millimeter-sized grains. Adv. Funct. Mater. 2013;**23**:198–203.

[27] Brown L et al. Polycrystalline graphene with single crystalline electronic structure. Nano Lett. 2014;**14**:5706.

[28] Faggio G, Capasso A, Messina G, Santangelo S, Dikonimos T, Gagliardi S, Giorgi R, Morandi V, Ortolani L and Lisi N. High temperature growth of graphene films on copper foils by ethanol chemical vapour deposition. J. Phys. Chem. C 2013;**117**:21569–76.

[29] Hao Y et al. The role of surface oxygen in the growth of large single-crystal graphene on copper. Science 2013;**342**:720.

[30] Gan L and Luo Z. Turning off hydrogen to realize seeded growth of subcentimeter single-crystal graphene grains on copper. ACS Nano 2013;**7:**9480.

[31] Li J, Wang X-Y, Liu X-R, Jin Z, Wang D and Wan L-J. Facile growth of centimeter-sized single-crystal graphene on copper foil at atmospheric pressure. J. Mater. Chem. C 2015;**3**:3530.

[32] Wang Y, Zheng Y, Xu X, Dubuisson E, Bao Q, Lu J and Loh K P. Electrochemical delamination of cvd grown graphene film: toward the recyclable use of copper catalyst. ACS Nano 2011;**5**:9927–93.

[33] Deng S, Berry V. Wrinkled, rippled and crumpled graphene: an overview of formation mechanism, electronic properties, and applications. Mater. Today 2016;**19**:197–212.

[34] Zhu W, Low T, Perebeinos V, Bol A, Zhu Y, Yan H, Tersoff J and Avouris P. Structure and electronic transport in graphene wrinkles. Nano Lett. 2012;**12**:3431–6.

[35] Duan W, Gong K and Wang Q. Controlling the formation of wrinkles in a single layer graphene sheet subjected to in-plane shear. Carbon 2011;**49**:3107–12.

[36] Park W. H. Electrical performance of chemical vapour deposition graphene on PET substrate tailored by Cu foil surface morphology. Eur. Phys. J. Appl. Phys. 2014;**67**:30701.

[37] Park W H, Jo I, Hong B H and Cheong H. Controlling the ripple density and heights: a new way to improve the electrical performance of CVD-grown graphene. Nanoscale 2016;**8**:9822.

[38] Kato R, Tsugawa K, Yamada T, Ishihara M and Hasegawa M. Improvement of multilayer graphene synthesis on copper substrate by microwave plasma process using helium at low temperatures. Japanese J. Appl. Phys. 2014;**53**:015505.

[39] Hussain S, Amade R, Moreno H and Bertran E. RF PECVD growth and nitrogen plasma functionalization of CNT son copper foil for electrochemical applications. Diam. Relat. Mater. 2014;**49**:55–61.

[40] Chaitoglou S, Pascual E, Bertran E and Andujar J L. Effect of a balanced concentration of hydrogen on graphene CVD growth. J. Nanomater. 2016;**2016**:9640935.

[41] Chaitoglou S and Bertran E. Effect of pressure and hydrogen flow in nucleation density and morphology of graphene bidimensional crystals. Mater. Res. Express 2016;**3**:075603.

[42] Raskova Z, Krcma F, Klima M and Kousal J. Diagnostic of plasma chemical treatment of archaeological artefacts. Czech. J. Phys. 2011;**52**:D927–32.

[43] Chang Y M, Leu J, Lin B H, Wang Y L and Cheng Y L. Comparison of H2 and NH3 treatments for copper interconnects. Adv. Mater. Sci. Eng. 2013;**7**:825195.

[44] Chen S, Brown L, Levendorf M et al. Oxidation resistance of graphene-coated Cu and Cu/Ni alloy. ACS Nano 2011;**5**:1321–7.

[45] Meca E, Lowengrub J, Kim H, Mattevi C and Shenoy V B. Epitaxial graphene growth and shape dynamics on copper: phase-field modeling and experiments. Nano Lett. 2013;**13**:5692–7.

[46] Hong J, Park M K, Lee E J, Lee D E, Hwang D S and Ryu S. Origin of new broad Raman D and G peaks in annealed graphene. Sci. Rep. 2013;**3**:2700.

[47] Wu P, Zhai X, Li Z and Yang J. Bilayer graphene growth via a penetration mechanism. J. Phys. Chem. C 2014;**118**:6201–6.

[48] Wood J D, Schmucker S W, Lyons A S, Pop E and Lyding J W. Effects of polycrystalline Cu substrate on graphene growth by chemical vapour deposition. Nano Lett. 2011;**11**:4547–54.

[49] Costa S D, Righi A, Fantini C, Hao Y, Magnuson C, Colombo L, Ruoff R S and Pimenta A. Resonant Raman spectroscopy of graphene grown on copper substrates. Solid State Commun. 2012;**152**:1317–20.

[50] Das A, Chakraborty B and Sood A. Raman spectroscopy of graphene on different substrates and influence of defects. Bull. Mater. Sci. 2008;**31**:579–84.

[51] Kim H, Mattevi C, Reyes Calvo M, Oberg J, Artiglia L, Agnoli S, Hirjibehedin C, Chhowalla M and Saiz E. Activation energy paths for graphene nucleation and growth on Cu. ACS Nano 2012;**6**:3614–23.

[52] Loginova E, Norman C B, Peter J F and Kevin F M. Evidence for graphene growth by C cluster attachment. New J. Phys. 2008;**10**:093026.

[53] Robinson V N E and Robins J L. Nucleation kinetics of gold deposited onto UHV cleaved surfaces of NaCl and KBr. Thin Solid Films 1974;**20**:155–75.

[54] Xing S, Wu W, Wang Y, Bao J and Pei S. Kinetic study of graphene growth: temperature perspective on growth rate and film thickness by chemical vapour deposition. Chem. Phys. Lett. 2013;**580**:62–6.

[55] Hayashi K, Sato S, Ikeda M, Kaneta C and Yokoyama N. Selective graphene formation on copper twin crystal. J. Am. Chem. Soc. 2012;**134**:12492.

[56] Lucchese M M, Stavale F, Martins Ferreira E H, Vilani C, Moutinho M V O, Capaz R, Achete C and Jorio A. Quantifying ion-induced defects and Raman relaxation length in graphene. Carbon 2010;**48**:1592–7.

[57] Eckmann A, Felten A, Verzhbitskiy I, Davey R and Casiraghi C. Raman study on defective graphene: effect of the excitation energy, type, and amount of defects. Phys. Rev. B 2013;**88**:035426.

[58] Cancado L G, Jorio A, Ferreira E H M, Stavale F, Achete C A, Capaz R B, Moutinho M V O, Lombardo A, Kulmala T S and Ferrari A C. Quantifying defects in graphene via Raman spectroscopy at different excitation energies. Nano Lett. 2011;**8**:3190.

[59] Paronyan T M, Pigos E M, Chen G and Harutyunyan A R. Formation of ripples in graphene as a result of interfacial instabilities. ACS Nano 2011;**5**:9619–27.

[60] Yoon D, Son Y and Cheong H. Negative thermal expansion coefficient of graphene measured by Raman spectroscopy. Nano Lett. 2011;**11**:3227–31.

[61] Tapasztó L, Dumitrica T, Kim S, Nemes-Incze P, Hwang C and Biró L P. Breakdown of continuum mechanics for nanometre-wavelength rippling of graphene. Nat. Phys. 2012;**8**:739–42.

[62] Lin Z, Ye X, Han J, Che Q, Fan P, Zhang H, Xie D, Zhu H and Zhong M. Precise control of the number of layers of graphene by picosecond laser thinning. Sci. Rep. 2015;**5**:11662.

[63] Frank O, Veravova J, Hol V, Kavan L and Kalbac M. Interaction between graphene and copper substrate: the role of lattice orientation. Carbon 2014;**68**:440–51.

[64] Rao R, Chen G, Arava L M, Kalaga K, Ishigami M, Heinz T F, Ajayan P M and Harutyunyan A R. Graphene as an atomically thin interface for growth of vertically aligned carbon nanotubes. Sci. Rep. 2013;**3**:1891.

[65] Mullins W W. Theory of thermal grooving. J. Appl. Phys. 1957;**28**:333.

[66] Wang Z, Weinberg G, Zhang Q, Lunkenbein T, Klein-Hoffmann A, Kurnatowska M, Plodinec M, Li Q, Chi L, Willinger M et al. Direct observation of graphene growth and associated copper substrate dynamics by in situ scanning electron microscopy. ACS Nano 2015;**9**:1506–19.

[67] Meng L, Su Y, Geng D, Yu G, Liu Y, Dou R, Nie J and He L. Hierarchy of graphene wrinkles induced by thermal strain engineering. Appl. Phys. Lett. 2013;**103**:251610.

[68] Westergren J, GrSnbeck H, Rosh A and Nordbolm S. Molecular dynamic simulations of metal cluster cooling and heating in noble gas atmosphere. Nanostruct. Mater. 1999;**12**:281–6.

[69] Goler S, Coletti C, Tozzini V, Piazza V, Mashoff T, Beltram F, Pellegrini V and Heun S. Influence of graphene curvature on hydrogen adsorption: Toward hydrogen storage devices. J. Phys. Chem. C 2013;**11**:11506–13.

[70] Troppenz G V, Gluba M A, Kraft M, Rappich J and Nickel N H. Strain relaxation in graphene grown by chemical vapour deposition. J. Appl. Phys. 2013;**114**:214312.